molecular pharmaceutics

THE UNIVERSITY OF NEWCASTLE AUSTRALIA

Subscriber access provided by University of Newcastle, Australia

Article

Design and Investigation of a [18F]-labeled Benzamide Derivative as a High Affinity Dual Sigma Receptor Subtype Radioligand for Prostate Tumor Imaging

Dongzhi Yang, Anthony Comeau, Wayne D. Bowen, Robert H. Mach, Brian D Ross, Hao Hong, and Marcian E. Van Dort

Mol. Pharmaceutics, **Just Accepted Manuscript** • DOI: 10.1021/acs.molpharmaceut.6b01020 • Publication Date (Web): 30 Jan 2017

Downloaded from http://pubs.acs.org on January 31, 2017

Just Accepted

"Just Accepted" manuscripts have been peer-reviewed and accepted for publication. They are posted online prior to technical editing, formatting for publication and author proofing. The American Chemical Society provides "Just Accepted" as a free service to the research community to expedite the dissemination of scientific material as soon as possible after acceptance. "Just Accepted" manuscripts appear in full in PDF format accompanied by an HTML abstract. "Just Accepted" manuscripts have been fully peer reviewed, but should not be considered the official version of record. They are accessible to all readers and citable by the Digital Object Identifier (DOI®). "Just Accepted" is an optional service offered to authors. Therefore, the "Just Accepted" Web site may not include all articles that will be published in the journal. After a manuscript is technically edited and formatted, it will be removed from the "Just Accepted" Web site and published as an ASAP article. Note that technical editing may introduce minor changes to the manuscript text and/or graphics which could affect content, and all legal disclaimers and ethical guidelines that apply to the journal pertain. ACS cannot be held responsible for errors or consequences arising from the use of information contained in these "Just Accepted" manuscripts.

ACS Publications

Molecular Pharmaceutics is published by the American Chemical Society. 1155 Sixteenth Street N.W., Washington, DC 20036

Published by American Chemical Society. Copyright © American Chemical Society. However, no copyright claim is made to original U.S. Government works, or works produced by employees of any Commonwealth realm Crown government in the course of their duties.

Design and Investigation of a [^{18}F]-labeled Benzamide Derivative as a High Affinity Dual Sigma Receptor Subtype Radioligand for Prostate Tumor Imaging

Dongzhi Yang[1,2], Anthony Comeau[3], Wayne D. Bowen[3], Robert H. Mach[4], Brian D. Ross[1], Hao Hong[1], Marcian E. Van Dort[1]

[1] Center for Molecular Imaging, Department of Radiology, University of Michigan – Ann Arbor, Michigan 48109-2200, United States

[2] Jiangsu Key Laboratory of New Drug Research and Clinical Pharmacy, Xuzhou Medical University, Xuzhou, Jiangsu 221004, China

[3] Department of Molecular Pharmacology, Physiology & Biotechnology, Brown University, Providence, RI 02912, United States

[4] Department of Radiology, University of Pennsylvania, Philadelphia, PA 19104, United States

* (H.H.) Fax: 1-734-763-5447; Tel: 1-734-615-4634; E-mail: hahong@med.umich.edu

(M.E.V) Fax: 1-734-763-5447; Tel: 1-734-615-2280; E-mail: mvandort@med.umich.edu

ABSTRACT: High overexpression of sigma (σ) receptors (σ_1 and σ_2 subtypes) in a variety of human solid tumors has prompted the development of σ receptor-targeting radioligands, as imaging agents for tumor detection. A majority of these radioligands to date, target the σ_2 receptor, a potential marker of tumor proliferative status. The identification of approximately equal proportions of both σ receptor subtypes in prostate tumors, suggests that a high affinity, dual σ receptor-targeting radioligand could potentially provide enhanced tumor targeting efficacy in prostate cancer. To accomplish this goal, we designed a series of ligands which bind to both σ receptor subtypes with high affinity. Ligand **3a** in this series, displaying optimal dual σ receptor subtype affinity (σ_1: 6.3 nM, σ_2: 10.2 nM) was radiolabeled with fluorine-18 (^{18}F) to give **[^{18}F]3a** and evaluated as a σ receptor-targeting radioligand in the mouse PC-3 prostate tumor model. Cellular assays with PC-3 cells demonstrated that a major proportion of **[^{18}F]3a** was localized to cell surface σ receptors, while ~10% of **[^{18}F]3a** was internalized within cells after incubation for 3.5 h. Serial PET imaging in mice bearing PC-3 tumors revealed that uptake of **[^{18}F]3a** was 1.6 ± 0.8, 4.4 ± 0.3, and 3.6 ± 0.6 %ID/g (% injection dose per gram) in σ receptor-positive prostate tumors at 15 min, 1.5 h, and 3.5 h post-injection, respectively (n = 3) resulting in clear tumor visualization. Blocking studies conducted with haloperidol (a non-selective inhibitor for both σ receptor subtypes) confirmed that the uptake of **[^{18}F]3a** was σ receptor-mediated. Histology analysis confirmed similar expression of σ_1 and σ_2 in PC-3 tumors which was significantly greater than its expression in normal organs/tissues such as liver, kidney, and muscle. Metabolite studies revealed that >50% of radioactivity in PC-3 tumors at 30 min post-injection represented intact **[^{18}F]3a**. Prominent σ receptor-specific uptake of **[^{18}F]3a** in prostate tumors and its subsequent clear visualization with PET imaging indicate potential utility for the diagnosis of prostate carcinoma.

KEYWORDS: Sigma receptors, positron emission tomography, PC-3 tumors, prostate cancer

1. INTRODUCTION:

Prostate cancer (PCa), the most diagnosed cancer in men, continues to present major challenges in its effective treatment, in part, due to staging inaccuracies and the inability to identify clinically important tumors. Noninvasive imaging modalities such as positron emission tomography (PET) and single photon emission computed tomography (SPECT) could provide fundamentally important information for early diagnosis, accurate staging, selection of optimum treatment and the monitoring of treatment efficacy of PCa. Consequently, there has been intense development in the past decade of new radioligands for the diagnostic imaging of PCa. PET imaging with [^{18}F]fluoromethylcholine (a choline analog involved in cell membrane phospholipid biosynthesis) is currently widely used for prostate tumor imaging. However, recent reports indicate that it has limited sensitivity and specificity for initial staging especially at low prostate specific antigen (PSA) levels.[1] Radioligands targeting the gastrin-releasing peptide receptor (GRPR), a member of the bombesin receptor family, radiolabeled with ^{68}Ga, ^{64}Cu, and ^{18}F have also been investigated as imaging radioligands for PCa. Among these, ^{68}Ga-RM2, ^{64}Cu-CB-TE2A-AR06, and ^{18}F-labeled BAY 864367 have shown promise in the detection of primary or recurrent PCa in early clinical trials.[2-5] More recently, prostate specific membrane antigen (PSMA) which displays high prostate tumor cell overexpression compared to normal tissues, has been reported as an important imaging biomarker for the diagnosis of PCa.[6] To date, small-molecule PSMA inhibitors, e.g. [^{68}Ga]HBED-CC-PSMA and [^{18}F]DCFPyl, show the most promise for diagnostic PET application.[7]

Radioligands which target sigma (σ) receptors present an alternative approach towards PCa imaging. Overexpression of σ receptors has been shown in many human solid tumors including melanoma, breast, lung, pancreas, prostate and those of neural origin.[8, 9] σ receptors comprise a distinct class of non-opiate, membrane-bound proteins which display high affinity

towards the small molecule ligands: 1,3-di-(2-tolyl) guanidine [DTG], (+)-3-(3-hydoxyphenyl)-*N*-(1-propyl)piperidine [(+)-3-PPP] or haloperidol.[10] The endogenous ligands for σ receptors and its exact function are yet unknown, however, two distinct σ receptor subtypes [sigma-1 (σ_1) and sigma-2 (σ_2)] have been identified based on their apparent molecular weights (σ_1 = 25 kDa; σ_2 = 21.5 kDa), tissue distribution patterns and ligand selectivity profiles.[11, 12] σ receptors are also normally present in many peripheral tissues (including liver, kidney, lung, endocrine glands) and the central nervous system.[12] The σ_1 receptor which has been cloned from a variety of tissues shows no sequence homology to any known mammalian proteins and has been identified as a unique ligand-operated chaperone protein localized primarily at the endoplasmic reticulum mitochondrion interface.[13] Progesterone receptor membrane component 1 (PGRMC1), a known biomarker of cell proliferation, has been suggested as a putative σ_2 receptor binding site[14] although recent reports have suggested that PGRMC1 and σ_2 receptors are two separate molecular entities.[15, 16] Tumor σ_2 expression has also been recognized as a potential receptor-based marker of the proliferative status of solid tumors.[14, 17] The pharmacology of σ receptor ligands has been extensively reviewed in the recent literature.[18-22]

Encouraging pre-clinical studies with σ receptor radioligands labeled with PET and SPECT radioisotopes have been reported for many cancers including melanoma,[23, 24] breast cancer,[25-27] and non-small cell lung cancer.[23] In contrast, there has been limited exploration of σ receptor radioligands for imaging prostate tumors with most reported studies to date focused on SPECT radioligand development.[28] A few examples of [^{11}C]-labeled σ receptor radioligands for prostate tumor imaging with PET have appeared in the literature. In one study, Colabufo and colleagues reported on a σ receptor ligand ([^{11}C]PB183) having good affinity towards both σ_1 and σ_2; however, *in vivo* studies with this radioligand have not been reported.[29] More recently, a

structurally similar σ receptor ligand ([^{11}C]PB28) with high affinity against σ_2 (K_i = 5.92 nM) was shown to display poor tumor uptake in mice bearing PC-3 prostate tumors.[30]

Typically, σ_2 subtype density overexpression exceeds that of σ_1 in most tumor types with the exception of neuroblastoma and prostate tumors where both subtypes are equally overexpressed.[8, 11, 31] This observation has been further confirmed with *in vitro* binding studies in a variety of prostate tumor cell lines including PC-3, LNCaP and DU-145.[8, 10, 11] The high density of total σ receptor tumor overexpression (e.g. approximately 1.8 million receptors per cell for DU-145 tumors)[10] suggests that σ receptor radioligands which bind to both subtypes could potentially provide enhanced tumor targeting compared to a radioligand which is selective towards a single subtype. To address this goal, our initial studies focused on the benzamide class of σ receptor ligands as a template for the design of a [^{18}F]-labeled dual σ receptor targeting radioligand for PET imaging of PCa. Fluorine-18 is an ideal radionuclide for PET imaging as its low positron emission energy (635 keV),[32] affords high quality images due to the short range of the emitted positrons.[33] Furthermore, its decay half-life (109.8 min) is compatible with the *in vivo* circulation time of most small-molecule ligands. We report herein on a series of (ω-fluoroalkylether)benzamides which display dual σ_1/σ_2 subtype binding affinity and initial biological and PET imaging studies with a high-affinity, [F-18]-labeled candidate in a mouse model of human PCa.

2. MATERIALS AND METHODS

2.1. Chemicals and Radiochemicals. Reagents and solvents were purchased from commercial suppliers and used without additional purification. 5-Bromosalicylic acid and 3-bromo-4-hydroxybenzoic acid were purchased from Alfa Aesar (Ward Hill, MA). 2-Fluoroethyl tosylate[34] and 3-fluoropropyl tosylate[35] were synthesized as previously reported. All other chemical reagents were obtained from Aldrich Chemical Co. (Milwaukee, WI). 2-[^{18}F]fluoroethyl tosylate

was purchased from the Cyclotron PET Facility, Department of Radiology, University of Michigan.

2.2. Chemical Characterization. Thin-layer chromatography (TLC) was performed using Analtech silica gel GF Uniplates (250 μm). TLC plates were visualized after development with either ultraviolet (UV) light or by spraying with phosphomolybdic acid reagent and subsequent heating. Flash column chromatography was performed on silica gel 60 (0.032 – 0.063 μm) purchased from EMD Millipore Corporation, Taunton, MA. Melting points were determined with a Thomas-Hoover melting point apparatus and are uncorrected. Elemental analyses were conducted by Atlantic Microlab Inc., Norcross, GA.

^{1}H NMR spectra were recorded on a Varian INOVA instrument operating at 400 MHz using $CDCl_3$, acetone-d_6 or DMSO-d_6 as solvents and tetramethylsilane (TMS) as internal standard. Chemical shifts (δ) and coupling constants (*J*) are reported in parts per million (ppm) and Hertz (Hz), respectively. High resolution mass spectral analyses were performed at the Department of Chemistry, University of Michigan, using either a VG-70-250-S mass spectrometer for electron impact (EI) and chemical ionization (DCI) modes, a Waters Autospec Ultima instrument with an electrospray interface for electrospray ionization (ESI) mode or a Waters Tofspec-2E run in reflectron mode. High performance liquid chromatography (HPLC) was performed using a Waters Breeze HPLC System (Waters Corporation, Milford, MA) equipped with a Waters 2487 Dual Wavelength Absorbance Detector. Radiochemical synthesis was performed using a TRACERlab FXFN Reactor module (GE Healthcare). HPLC analysis was conducted at ambient temperature using a Waters Sunfire C-18 column (4.6 x 250 mm), 5 μm particle, with 0.1% TFA in H_2O (component A) and 0.1% TFA in CH_3CN (component B) solvent mixtures as eluent with UV absorbance monitoring at 254 and 280 nm. HPLC runs were conducted using a solvent gradient of 10%B to 90%B over 25 min at a flow rate of 1 mL/min.

Radioactivity was monitored with a Bioscan Flow Count FC-3300 NaI/PMT Radiodetector (Bioscan, Inc., Washington, DC) equipped with a 1.5" x 1.5" NaI(Tl) crystal. LC-MS/MS analysis was conducted at ambient temperature using a Waters XBridge C-18 column (4.6 x 50 mm), 5 μm particle, with 0.1% HCOOH in H_2O (component A) and 0.1% HCOOH in CH_3CN (component B) solvent mixtures as eluent. HPLC runs for liver microsomal assays were conducted with 5 μL injections at a flow rate of 1 mL/min using the following solvent gradient (%B): 0 min: 2%, 0.5 min: 2%, 2.5 min: 90%, 3.5 min: 90%, 3.6 min: 2%, 5.6 min: 2%. Radioactivity measurements were obtained with a Capintec CRC-15W Radioisotope Dose Calibrator (Ramsey, NJ).

2.3. Radioligand Design Strategy

Previously described benzamide compound structures with selectivity towards a single σ receptor subtype (**Figure 1**) were utilized as templates for the design of potential dual σ receptor subtype binding radioligands. Compounds 4-IPAB[10] and PIMBA[10] display nanomolar σ_1 affinity and moderate selectivity (17- to 80-fold) over σ_2 whereas the 1,2,3,4-tetrahydroisoquinoline analogs (**8**, **9)** are high-affinity, σ_2 selective (σ_2/ σ_1 ratio >1200) ligands (**Figure 1**).[36] Comparison of these two classes of chemical structures suggested that inclusion of lipophilic ether substituents at the 2-position of the aromatic ring in core structures such as 4-IPAB and PIMBA could lead to an improvement in its σ_2 affinity. Accordingly, a series of benzamide derivatives incorporating either 2- or 4-fluoroalkylated ether linkers were initially synthesized for screening of their σ_1 and σ_2 receptor binding affinities for investigation as potential radiofluorinated dual SR subtype binding radioligands.

2.4. Synthesis of 5-bromo-2-hydroxy-*N*-{2-(piperidin-1-yl)ethyl}benzamide (2). A stirred suspension of 5-bromosalicyclic acid (**1**) (3.0 g, 13.8 mmol) in anhydrous $CHCl_3$ (120 mL) was treated with $SOCl_2$ (4.9 g, 41.5 mmol) and DMF (0.2 mL) and refluxed for 3 h. The mixture was

concentrated under reduced pressure to afford the crude acid chloride as a yellow solid. A suspension of the acid chloride in a mixture of toluene (70 mL) and DMF (4 mL) was added dropwise to a solution of *N*-(2-aminoethyl)piperidine (2.12 g, 16.6 mmol) and Et_3N (3.07 g, 30.4 mmol) in toluene (70 mL) and stirred at ambient temperature for 3 h. The mixture was washed with brine, H_2O and dried (Na_2SO_4). Purification by silica-gel flash chromatography (5% CH_3OH in $CHCl_3$ with 1% added NH_4OH) gave 2.8 g (62% overall yield) of the title compound as a cream amorphous solid: ^{1}H NMR (acetone-d_6): δ 8.29 (br s, 1H), 7.91 (d, J = 2.5 Hz, 1H), 7.51 (dd, J = 8.8 Hz , 2.3 Hz, 1H), 6.88 (dd, J = 8.8 Hz , 3.1 Hz, 1H), 3.54 – 3.52 (m, 2H), 2.58 – 2.56 (m, 2H), 2.54 – 2.45 (m, 4H), 1.58 – 1.52 (m, 4H), 1.43 – 1.42 (m, 2H). HRMS [ESI with Na^+ added]: Calculated for $C_{14}H_{20}N_2O_2Br$ [M + H^+]: 327.0708. Observed: 327.0710. Anal. ($C_{14}H_{19}N_2O_2Br$): C, H, N. HPLC: t_R (chemical purity) = 11.7 min (99.9%).

2.5. Synthesis of 5-Bromo-2-(2-fluoroethoxy)-*N*-{2-(piperidin-1-yl)ethyl}benzamide (3a). A stirred solution of **2** (0.2 g, 0.61 mmol) in anhydrous CH_2Cl_2 (9 mL) was treated with a solution of tetrabutylammonium hydroxide (1M in CH_3OH, 0.67 mL, 0.67 mmol) and concentrated under reduced pressure after 15 min. Residual water was removed by treatment of the residue thrice with 5 mL portions of anhydrous CH_3CN and concentration under reduced pressure. The residue was reconstituted in anhydrous DMF (5 mL), treated with a solution of 2-fluoroethyl tosylate (0.16 g, 0.73 mmol) in DMF (1 mL) and heated at 65 – 70 ^{0}C for 3 h. The crude mixture was partitioned between EtOAc and brine and the organic layer was washed with brine, H_2O and dried (Na_2SO_4). Silica-gel flash chromatography (gradient of 3% - 10% CH_3OH in CH_2Cl_2 with 1% added NH_4OH) of the crude product mixture provided 0.13 g (57%) of material which was recrystallized from hexane:EtOAc (1:1) to give a white crystalline solid: mp 101 – 102 ^{0}C; ^{1}H NMR ($CDCl_3$): δ 8.33 (d, J = 2.8 Hz, 1H), 8.10 (br s, 1H), 7.51 (dd, J = 8.6 Hz, 2.6 Hz, 1H), 6.83 (d, J = 8.8 Hz, 1H), 4.86 (dt, $J_{H\text{-}F}$ = 47.4 Hz, 4.1 Hz, 2H), 4.35 (dt, $J_{H\text{-}F}$ = 27.2 Hz, 4.1 Hz, 2H),

3.59 – 3.55 (m, 2H), 2.53 (t, J = 6.2 Hz, 2H), 2.42 (br s, 4H), 1.61 – 1.55 (m, 4H), 1.48 – 1.45 (m, 2H). HRMS [ESI with Na^+ added]: Calculated for $C_{16}H_{23}N_2O_2BrF$ [M+H^+]: 373.0927. Observed: 373.0926. Anal. ($C_{16}H_{22}N_2O_2BrF$): C, H, N. HPLC: t_R (chemical purity) = 12.0 min (99.9%, **Figure S1**).

2.6. 5-Bromo-2-(3-fluoropropoxy)-*N*-{2-(piperidin-1-yl)ethyl}benzamide (3b). A similar procedure to that shown for **3a** above provided 0.18 g (61%) of the title compound **3b** which was recrystallized from hexane:EtOAc (1:1) to give a white crystalline solid: mp 64 – 66 ^{0}C; ^{1}H NMR ($CDCl_3$): δ 8.31 (d, J = 2.5 Hz, 1H), 8.09 (br s, 1H), 7.50 (dd, J = 8.8 Hz, 2.7 Hz, 1H), 6.86 (d, J = 8.8 Hz, 1H), 4.66 (dt, J_{H-F} = 47.1 Hz, 5.5 Hz, 2H), 4.27 (t, J = 6.1 Hz, 2H), 3.58 – 3.54 (m, 2H), 2.51 (t, J = 6.1 Hz, 2H), 2.41 – 2.24 (overlapping m, 6H), 1.60 – 1.54 (m, 4H), 1.48 – 1.45 (m, 2H). HRMS [ESI with Na^+ added]: Calculated for $C_{17}H_{25}N_2O_2BrF$ [M+H^+]: 387.1078. Observed: 387.1078. Anal. ($C_{17}H_{24}N_2O_2BrF$): C, H, N. HPLC: t_R (chemical purity) = 12.9 min (99.9%, **Figure S1**).

2.7. Synthesis of 3-Bromo-4-hydroxybenzoic acid succinimidyl ester (5). A stirred suspension of 3-bromo-4-hydroxybenzoic acid (**4**) (2.36 g, 10.9 mmol) and *N*,*N*-disuccinimidyl carbonate (3.1 g, 12 mmol) in anhydrous CH_3CN (100 mL) was treated dropwise with pyridine (0.97 mL, 0.95 g, 12 mmol) and stirred at ambient temperature for 18 h. The mixture was concentrated under reduced pressure and purified by silica-gel flash chromatography (gradient of 30% - 60% EtOAc in hexane) to give 3 g (88%) of material which was recrystallized from hexanes:EtOAc (1:1) to give a white crystalline solid: mp 171 – 172 ^{0}C; ^{1}H NMR (DMSO-d_6): δ 11.82 (br s, 1H), 8.15 (d, J = 2.1 Hz, 1H), 7.96 (dd, J = 8.6 Hz, 2.1 Hz, 1H), 7.15 (d, J = 8.6 Hz, 1H), 2.88 (s, 4H). HRMS [ESI with Na^+ added]: Calculated for $C_{11}H_8NO_5BrNa$ [M + Na^+]: 335.9478. Observed: 335.9472. Anal. ($C_{11}H_8NO_5Br$): C, H, N.

2.8. Synthesis of 3-bromo-4-hydroxy-*N*-{2-(piperidin-1-yl)ethyl}benzamide (6). A stirred suspension of **5** (2.31 g, 7.35 mmol) in anhydrous CH_2Cl_2 (80 mL) was treated by dropwise addition with a solution of *N*-(2-aminoethyl)piperidine (0.94 g, 7.35 mmol) in CH_2Cl_2 (5 mL) and stirred for 3 h. The crude product was purified by silica-gel flash chromatography (20% CH_3OH in CH_2Cl_2 with 1% added NH_4OH) to give 1.7 g (71%) of the title compound **6** as a white amorphous solid: ^{1}H NMR (acetone-d_6): δ 8.03 (d, J = 2.1 Hz, 1H), 7.73 (dd, J = 8.4 Hz, 2.1 Hz, 1H), 7.59 (br s, 1H), 7.03 (d, J = 8.5 Hz, 1H), 3.49 (doublet, J = 6.4 Hz, 1H), 3.46 (doublet, J = 6.4 Hz, 1H), 2.53 (t, J = 6.5 Hz, 2H), 2.45 (m, 4H), 1.58 – 1.53 (m, 4H), 1.45 – 1.41 (m, 2H). HRMS [ESI]: Calculated for $C_{14}H_{20}N_2O_2Br$ [M + H^+]: 327.0703. Observed: 327.0712. Anal. ($C_{14}H_{19}N_2O_2Br$): C, H, N. HPLC: t_R (chemical purity) = 8.7 min (99.9%).

2.9. 3-Bromo-4-(2-fluoroethoxy)-*N*-{2-(piperidin-1-yl)ethyl}benzamide (7a). A similar procedure to that shown for **3a** above provided the title compound in 90% yield as a white crystalline solid: mp 108 – 109 ^{0}C [hexane:EtOAc (1:1)]; ^{1}H NMR ($CDCl_3$): δ 8.01 (d, J = 2.2 Hz, 1H), 7.74 (dd, J = 8.6 Hz, 2.1 Hz, 1H), 6.96 (br s, 1H), 6.94 (d, J = 8.6 Hz, 1H), 4.82 (dt, $J_{H\text{-}F}$ = 47.2 Hz, 4.3 Hz, 2H), 4.33 (dt, $J_{H\text{-}F}$ = 27.0 Hz, 4.1 Hz, 2H), 3.54 – 3.50 (m, 2H), 2.58 (t, J = 5.9 Hz, 2H), 2.47 (br s, 4H), 1.65 – 1.60 (m, 4H), 1.51 – 1.48 (m, 2H). HRMS [ESI^+]: Calculated for $C_{16}H_{23}N_2O_2BrF$ [M+H^+]: 373.0921. Observed: 373.0919. Anal. ($C_{16}H_{22}N_2O_2BrF$): C, H, N. HPLC: t_R (chemical purity) = 11.7 min (99.3%, **Figure S1**).

2.10. 3-Bromo-4-(3-fluoropropoxy)-*N*-{2-(piperidin-1-yl)ethyl}benzamide (7b). A similar procedure to that shown for **3b** above provided the title compound in 89% yield as a colorless viscous oil; ^{1}H NMR ($CDCl_3$): δ 8.00 (d, J = 2.1 Hz, 1H), 7.71 (dd, J = 8.6 Hz, 2.4 Hz, 1H), 6.93 (d, J = 8.6 Hz, 1H), 6.85 (br s, 1H), 4.71 (dt, $J_{H\text{-}F}$ = 46.9 Hz, 5.7 Hz, 2H), 4.21 (t, J = 6.0 Hz, 2H), 3.52 – 3.48 (m, 2H), 2.54 (t, J = 6.0 Hz, 2H), 2.43 (br s, 4H), 2.31 – 2.18 (overlapping m,

2H), 1.63 – 1.57 (m, 4H), 1.50 – 1.47 (m, 2H). HRMS [ESI$^+$]: Calculated for $C_{17}H_{25}N_2O_2BrF$ [M+H$^+$]: 387.1078. Observed: 387.1080. Anal. ($C_{17}H_{24}N_2O_2BrF$): C, H, N. HPLC: t_R (chemical purity) = 12.9 min (98.8%, **Figure S1**).

2.11. *In vitro* σ_1 Binding Assays. These assays were conducted as previously reported.[10] In brief, guinea pig brain membrane homogenates (300 – 500 μg of total protein) were incubated with 3 nM [^{3}H]-(+)-pentazocine (51.7 Ci/mmol) in 0.5 mL of 50 mM Tris-HCl, pH 8.0, at 25 ^{0}C for 120 min. Test ligands were added in concentrations ranging from 10^{-4} to 10^{-12} M. Assays were terminated by the addition of 5 mL of ice-cold 10 mM Tris-HCl (pH 8.0) and filtered through glass fiber filters and filters washed twice with 5 mL of ice-cold 10 mM Tris HCl (pH 8.0). Filters were soaked in 0.5% polyethyleneimine for at least 30 min at 25 ^{0}C prior to use. Non-specific binding was determined in the presence of 10 μM haloperidol. IC_{50} values were determined using the computerized iterative curve-fitting program GraphPad. K_i values were calculated from the IC_{50} values using the Cheng-Prussoff equation. Protein concentration was determined by the Lowry method.

2.12. *In vitro* σ_2 Binding Assays. These assays were conducted by incubation of rat liver membrane homogenates (150 – 200 μg of total protein) with 3 nM [^{3}H]DTG (39.4 Ci/mmol)in the presence of 1 μM dextrallorphan (to mask σ_1 sites). Non-specific binding was determined in the presence of 10 μM haloperidol. All other procedures were identical to those described for the σ_1 receptor binding assay described above.

2.13. Mouse Liver Microsomal Assay. This assay was conducted by incubation of **3a** with a mouse liver microsomal preparation as follows: 10 μL of microsomal mixture (20 mg/mL) was diluted with 366 μL of 0.1M phosphate buffer (3.3 mM $MgCl_2$) followed by the addition of 4 μL of 100 μM stock solution of **3a** and Verapamil (positive control). The incubation mixture was pre-warmed to 37 ^{0}C for 3 min. The reaction was initiated by treatment with 20 μL of a NADPH-

generating system consisting of 4 mg of NADPH in 240 μL of 0.1M phosphate buffer (3.3 mM $MgCl_2$). The final concentration of test compounds in the reaction system was 1 μM. At designated time intervals (0, 5, 10, 15, 30, 45 and 60 min), 30 μL aliquots of the reaction solution were removed by pipette and quenched by the addition of 9 volumes of cold CH_3CN containing 10 nM of CE302 as internal standard. The incubation solution was centrifuged at 3500 g for 15 min to precipitate protein and the supernatant was used for LC-MS/MS analysis.

2.14. Radiosynthesis of [^{18}F]3a. The radiosynthesis of **[^{18}F]3a** was conducted by reaction of the tetrabutylammonium phenolate salt of **2** with 2-[^{18}F]fluoroethyl tosylate **(Scheme 3).** In brief, a solution of **2** (2.3 mg, 6.7 μmoles) in 1 mL of CH_3CN and tetrabutylammonium hydroxide solution (1M in CH_3OH, 6.7 μl, 6.7 μmoles) were added sequentially to the FXFN reactor module and evaporated to dryness at 45 ^{0}C with a helium stream under vacuum. [^{18}F]fluoroethyl tosylate was eluted from an Oasis C-18 cartridge using anhydrous CH_3CN (1 mL) into the reactor containing the anhydrous tetrabutylammonium salt precursor. The mixture was heated at 90 ^{0}C for 10 min, then cooled to 45 ^{0}C, diluted with water (3 mL) and injected onto a semi-preparative reversed phase HPLC column (Phenomenex Gemini C-18, 5 μm (10 mm × 250 mm)). Product purification was conducted under isocratic conditions with a mobile phase of 28% acetonitrile in water with 0.1% added TFA at a flow rate of 4.0 mL/min with UV absorbance (254 nm) and radioactivity detection. The radioactive fraction corresponding to **[^{18}F]3a** ($11.2 < t_R < 12.4$ min) was collected in a flask containing sterile water (25 mL) and eluted through a pre-activated (methanol, H_2O) Empore C18 XDB-XC cartridge. The C18 cartridge was rinsed with additional water (5 mL) and the trapped, purified radiolabeled product was eluted from the cartridge with ethanol (0.3 mL) followed by 0.9% saline (3 mL). The formulated solution was filtered using a sterile Millipore GV 0.22 μm filter into a 10 mL vial. Product formulations in saline containing 5% ethanol by volume were subsequently used for animal studies.

Confirmation of product identity was conducted using HPLC analysis by co-injection with the authentic unlabeled standard **3a** (t_R = 11.6 ± 0.3 min; n = 8).

2.15. Determination of Radiochemical Purity and Specific Activity. Chemical and radiochemical purity estimates were obtained on the same sample by HPLC analysis. Specific activity estimates were determined by comparison of the UV absorbance peak area corresponding to the radioligand on the HPLC chromatogram with a standard calibration curve relating mass (0.5 – 20 μg) to UV absorbance peak area (254 nm).

2.16. Cell Internalization/Efflux Studies. Cell uptake/internalization assays were conducted with **[^{18}F]3a** using PC-3 cells to further characterize its cell interaction kinetics during the time frame of PET imaging (5 min – 3.5 h). PC-3 cells were washed thrice with cold PBS, detached by a cell dissociation buffer (Life Technologies) for 15 min, and re-suspended in PBS at a final concentration of 2 × 10^6/mL. The cells were then divided into two portions. One portion of cells was incubated with 10^5 cpm/mL (cpm: counts per minute) of **[^{18}F]3a.** At serial time points (5 min, 15 min, 0.5, 1.0, 1.5, 2.0, 2.5, and 3 h) an aliquot (0.3 mL) of cell suspension was removed and centrifuged for pellet isolation. After repeated washing with PBS, cell pellets were re-suspended in 0.01 M sodium citrate, 0.14 M NaCl buffer (pH = 2) for 2 min at room temperature and then centrifuged. The amount of internalized **[^{18}F]3a** was calculated by assay of the radioactivity that remained associated with the cells after the wash with pH 2 buffer, while the radioactivity in the supernatant represented cell surface-associated **[^{18}F]3a**. An additional portion of PC-3 cells was incubated with 10^5 cpm/mL of **[^{18}F]3a** for 0.5 h (when maximal internalization was achieved). The cell suspension was then centrifuged and washed with PBS repeatedly. PC-3 cells were re-suspended in PBS at a density of 2 × 10^6/mL, and 0.3 mL of the cell suspension was removed from the culture and centrifuged at serial time points (5 min, 15 min, 0.5, 1.0, 1.5,

2.0, 2.5, and 3 h). Radioactivity measured in the supernatant represented the efflux of **[^{18}F]3a** from the cells. All measurements were carried out in triplicate.

2.17. Tumor Model and PET Imaging. All animal studies were conducted under an animal use protocol approved by the University Committee on Use and Care of Animals (UCUCA) at the University of Michigan. Tumors were established by subcutaneous injection of 2×10^6 of PC-3 cells suspended in 100 μL of a 1:1 mixture of PBS and Matrigel (BD Biosciences, Franklin Lakes, NJ) into the front flank of male nude mice (6-10 weeks old, 20 – 25 g) purchased from Charles River Laboratories. Tumor size was monitored every other day and mice were subjected to *in vivo* experiments when the tumor diameter reached 5-8 mm (typically 4-6 weeks after inoculation).

PET imaging was performed on a Siemens Inveon PET/CT small animal scanner (Siemens Medical Solutions, Knoxville, TN) equipped with a computer controlled bed and operated in three-dimensional list mode. Each tumor-bearing mouse was injected with 5-10 MBq of **[^{18}F]3a** via the tail vein and subjected to static PET scans (40 million events per scan, 350 – 750 keV energy window) at various time points post-injection (p.i.). Mice were anesthetized prior to scanning with 2% (v/v) isoflurane and maintained thereafter with 1 – 2% isoflurane (v/v). PET images were reconstructed with 3-Dimensional Ordered-Subsets Expectation Maximization (3D-OSEM) algorithms without CT attenuation correction and analyzed using Siemens IRW software. Circular regions of interest (ROI) were drawn around tumor/tissue (or regions of interest of the highest uptake within tumor/tissue). Regional uptake of radioactivity was decay-corrected to the time of injection and tumor uptake (units of % injected dose per gram [%ID/g]) was calculated as the activity concentration within an ROI normalized by the ratio of the injected dose and the animal weight. Radioactivity tissue concentration data obtained from these studies were combined to generate composite time-activity curves for selected tissues.

Separate groups of three mice were subjected to dynamic PET scans (10 frames with 2 min per time frame) immediately after intravenous injection of **[^{18}F]3a** to determine its *in vivo* circulation time.

2.18. Tissue Biodistribution Studies. Biodistribution studies were carried out to correlate the radiotracer uptake based on PET imaging with the quantitative radioactivity distribution data obtained in PC-3 tumor-bearing mice. Following PET imaging at 3.5 h p.i., mice were euthanized and blood, tumor, and major organs/tissues were collected and wet-weighed. The radioactivity in each sample was measured using a WIZARD^2 automatic gamma-counter (Perkin-Elmer) and recorded as %ID/g (mean ± SD). Tumor, liver, spleen, and muscle were also frozen for further histological analysis. A separate group of PC-3 tumor-bearing mice (n = 3) were injected via the tail vein with 0.5 – 1 MBq of **[^{18}F]3a** and sacrificed at 1.5 h after radioligand injection to compare its early organ distribution profile with the data acquired in PET studies. All radioactivity measurements were corrected for radioisotope decay.

2.19. Tissue Radiometabolite Assays. Tumor, liver and blood were analyzed for radiometabolites of **[^{18}F]3a** at 5 min and 30 min after intravenous injection. Mice (n = 2 per time point) were injected with **[^{18}F]3a** (6 – 10 MBq) and euthanized by decapitation under isoflurane anesthesia at selected time intervals. Tissues were minced, homogenized in 400 μL of ice-cold CH_3CN:H_2O (95:5) and centrifuged at 12,000 g for 10 min. The supernatant and pellet were separated and assayed with a gamma-counter to determine the extraction efficiency (extraction efficiency >95%). The supernatant was filtered, concentrated by evaporation with a nitrogen stream and aliquots were spiked with nonradioactive **3a** prior to HPLC analysis. The percentage of intact radioligand and metabolites were calculated as the % ratio of their respective HPLC radiochromatogram peak areas to the total peak area.

2.20. Statistical Analysis

Data is reported as mean ± standard deviation (SD). Differences in tissue uptake in blocking studies were evaluated for statistical significance with a paired 2-tailed Students *t* test using Microsoft Excel. P values < 0.05 were considered as statistically significant.

3. RESULTS

3.1. Synthetic Chemistry. Synthesis of the 2-(ω-fluoroalkyl)ether substituted compounds (**3a**, **3b**) were conducted as shown in **Scheme 1** by initial conversion of 5-bromosalicylic acid (**1**) to the acid chloride using thionyl chloride followed by treatment with *N*-(2-aminoethyl)piperidine to give the 2-hydroxybenzamide analog **2**. Treatment of the tetrabutylammonium phenolate salt of **2** with the appropriate ω-fluoroalkyl tosylate in DMF at 65 ^{0}C provided compounds **3a** and **3b** in 57 – 61% yields. Synthesis of the 4-(ω-fluoroalkyl)ether substituted compounds (**7a**, **7b**) were conducted using a different approach **(Scheme 2)** as we were unsuccessful in our attempts to convert 3-bromo-4-hydroxybenzoic acid (**4**) to its corresponding 4-hydroxybenzamide derivative (**6**) by the previous method. Compound **6** was subsequently synthesized by initial conversion of **4** to the corresponding succinimidyl ester (**5**) followed by treatment with *N*-(2-aminoethyl)piperidine (**Scheme 2**). Alkylation of the tetrabutylammonium phenolate salt of **6** with the appropriate ω-fluoroalkyl tosylate as described previously gave the final compounds **7a** and **7b** in 89 – 90% yields.

3.2. σ Receptor Binding

The binding affinities of new benzamide ligands for σ receptor subtypes were determined using *in vitro* competitive binding assays. These data (expressed as inhibition constants, K_i) are presented in **Table 1**. All four fluoroalkylether substituted benzamide derivatives displayed nanomolar binding affinities towards both σ receptor subtypes. Analog **3a** bearing a 2-fluoroethoxy substituent at the 2-position of the aromatic ring showed the highest σ receptor binding affinity in the series (σ_1 = 6.26 nM; σ_2 = 10.2 nM). However, shifting the 2-fluoroethoxy

substituent to the 4 position (analog **7a**) resulted in a 6- and 4-fold reduction in its σ_1 and σ_2 affinity, respectively. In contrast, the 3-fluoropropylether substituent was moderately well tolerated at the 4-position (analog **7b**: σ_1 = 23.3 nM; σ_2 = 28.3 nM) but relatively less tolerated at the 2-position (analog **3b**) resulting in a 9-fold reduction in its σ_1 and σ_2 affinity. The phenol intermediates **2** and **6** were devoid of σ receptor binding affinity.

3.3. Mouse Liver Microsomal Metabolism

The rate of metabolism of **3a** in the presence of mouse liver microsomes was determined by quantification of intact **3a** using LC-MS/MS analysis. The half-life ($T_{1/2}$) of metabolic degradation of **3a** was determined to be 5.94 min (**Table S2**).

3.4. Radiochemistry

Radiosynthesis was completed in approximately 55 min and afforded decay-corrected radiochemical yields of **[^{18}F]3a** of 35 - 50% (n = 12) based on initial activity of 2-[^{18}F]fluoroethyl tosylate, with an average specific activity of 226 GBq/μmol (n = 6). The radiochemical and chemical purity of the final product was ≥99% by HPLC analysis (t_R = 11.6 ± 0.3 min; n = 8).

3.5. Cell Uptake Studies

Prior to initiating *in vivo* experiments, we examined the cell interaction kinetics (internalized, surface-bound, and efflux) between **[^{18}F]3a** and σ receptor-positive PC-3 cells and these results are shown in **Figure 2**. As seen from this data, the majority of **[^{18}F]3a** was associated with the cell membrane (**Panel A**) as compared to the cell-internalized component (peak values at 15 min post-incubation, 13033.0 ± 593.1 Bq/10^6 cells). In comparison, the internalized fraction of **[^{18}F]3a** (**Panel B**) was significantly lower (peak values at 30 min post-incubation, 1058.8 ± 593.1 Bq/10^6 cells). We estimate that ~ 10% of **[^{18}F]3a** was internalized within PC-3 cells, possibly mediated via σ receptor internalization. Cell efflux studies (**Panel C**)

also revealed that ~33% of **[^{18}F]3a** was effluxed from PC-3 cells after cell internalization (at 3 h post-incubation).

3.6. *In Vivo* PET Imaging Studies

The *in vivo* circulation half-life of **[^{18}F]3a** was determined to be 67.3 ± 15.7 s (**Figure S2**). Based on the short circulation time, PET imaging was conducted at 15 min, 1.5 h, and 3.5 h following intravenous injection of **[^{18}F]3a** into PC-3 tumor bearing mice. Reconstructed coronal slices containing PC-3 tumors are shown in **Figure 3A**. As seen from the mouse PET image data, **[^{18}F]3a** undergoes rapid excretion via both renal and hepatobiliary pathways (**Figure 3B**), while also displaying increasing tumor accumulation with time compared to non-target organs such as liver, kidney and spleen which resulted in clear visualization of PC-3 tumors. **[^{18}F]3a** showed a maximum tumor uptake of 4.4 ± 0.3 %ID/g at 1.5 h post-injection with corresponding tumor uptake values of 1.6 ± 0.8, and 3.6 ± 0.6 %ID/g at 15 min and 3.5 h p.i., respectively (**Figure 3A & B**). To further investigate the specificity of **[^{18}F]3a** towards σ receptors, "blocking" experiments were conducted by co-injection of the high-affinity, non-selective σ receptor ligand haloperidol (10 μmol/kg[37]) with **[^{18}F]3a** into tumor-bearing mice (n = 3). Haloperidol administration reduced the tumor uptake of **[^{18}F]3a** at both 1.5 h and 3.5 h p.i. ($p < 0.05$) – the uptake was 1.2 ± 0.2, 3.3 ± 0.3, and 2.0 ± 0.2 %ID/g at 15 min, 1.5 h, and 3.5 h p.i., respectively (**Figure 3B, C & D**) confirming that tumor uptake was σ receptor-mediated.

3.7. *Ex Vivo* Studies (Organ Distribution & Histology)

Mice were euthanized following the terminal PET scans at 3.5 h p.i., for biodistribution studies to corroborate the PET imaging data. These studies demonstrate that accumulation of **[^{18}F]3a** in PC-3 tumors was higher compared to other organs/tissues (e.g. liver, kidney, and spleen) (**Figure 4A**), affording optimal contrast for tumor detection with PET. In the haloperidol "blocking" group, a faster clearance of **[^{18}F]3a** was detected (statistical difference in blood,

heart, lung, liver, tumor, and brain), an observation likely attributable to decreased availability of σ_1 and σ_2 receptors due to occupancy by haloperidol. Overall, **[^{18}F]3a** demonstrates good tumor contrast in PC-3 tumor-bearing mice with a tumor-to-muscle ratio of 4.0 ± 0.3 at 3.5 h p.i. (n = 3), compared with 1.8 ± 0.2 for the haloperidol "blocking" group (n = 3). Additionally, biodistribution studies conducted on a separate batch of mice (n = 3) at 1.5 h p.i. (at peak tumor uptake) after radioligand administration revealed an organ distribution pattern consistent with that observed in the PET images (**Figure 4A**), and the tumor-to-muscle ratio at this time was 3.1 ± 0.6 (n = 3).

Immunofluorescence staining for σ_1 and σ_2 receptor expression was conducted in mouse PC-3 tumor sections as well as selected organs/tissues. These studies revealed prominent expression of both σ receptor subtypes in PC-3 tumor sections (**Figure 4B**). Furthermore, substantially weaker fluorescence was observed in liver, kidney and muscle.

3.8. Radiometabolite Analysis

HPLC analysis of tumor and blood radioactivity at 5 min post-injection showed that >99% of the total extracted radioactivity was associated with intact **[^{18}F]3a** (t_R = 11.8 min). However, at 30 min post-injection the corresponding values for tumor and blood had declined to 52% and 24%, respectively, and the remaining radioactivity was associated with a single polar metabolite eluting at t_R = 3.8 min. In the case of liver, intact **[^{18}F]3a** comprised 46% and 67% of the total radioactivity at 5 min and 30 min post-injection, respectively, and the remaining radioactivity was a single polar metabolite (t_R = 3.8 min) as seen previously.

4. DISCUSSION

Our design strategy based on the benzamide compound structure as template led to the discovery of several ω-fluoroalkylether derivatized benzamides displaying potent affinity

towards both σ receptor subtypes. An important advantage of the benzamide core structure is its conformational flexibility, low to moderate lipophilic properties and ease of structural modification for radiolabel incorporation. Radioligand lipophilicity as measured by its log P value (or log D for ionizable compounds) impacts its plasma protein bound fraction, ability to cross cell membranes and non-specific binding. In general, high radioligand lipophilicity leads to increased non-specific binding resulting in a lowered signal-to-background contrast ratio. Log P or (log D) values within the 1 - 3 range have been proposed as desirable for candidate radioligands.[38, 39] The fluorinated benzamides in our series display clog P(D) values (**Table 1**) within this optimal range for *in vivo* radioligands that demonstrate reduced non-specific binding. *In vitro* receptor binding studies showed that the four fluorinated benzamide derivatives in the series displayed high to moderate dual σ receptor binding affinity (6.3 nM < K_i < 92.9 nM) confirming our design hypothesis (**Table 1**). We subsequently selected analog **3a** for [^{18}F]-labeling and additional *in vivo* evaluation based on its optimal dual SR binding affinity (σ_1 = 6.26 nM; σ_2 = 10.2 nM).

PET imaging studies with **[^{18}F]3a** showed increasing tumor accumulation of radioactivity with time with a peak tumor uptake of 4.4 %ID/g at 1.5 h post-injection. Moreover, rapid excretion of radioactivity via both renal and hepatobiliary pathways from 1 – 3.5 h post-injection resulted in clear tumor visualization in the PET images during this time interval. Additionally, biodistribution studies conducted on PC-3 tumor bearing mice at 1.5 h (at peak tumor uptake) and 3.5 h after radioligand administration revealed an organ distribution pattern consistent with that seen with the PET image data. We used haloperidol which displays high affinity towards both σ_1 (K_i = 4.95 nM) and σ_2 (K_i = 20.7 nM)[40] receptor subtypes for pharmacological blockade studies to demonstrate *in vivo* σ receptor specificity of **[^{18}F]3a**. Co-injection of **[^{18}F]3a** with haloperidol (1 mg/Kg) resulted in a significant reduction (45%) in tumor radioactivity at 3.5 h

post-injection demonstrating that tumor uptake was σ receptor mediated. These results were also confirmed by the biodistribution data wherein haloperidol administration showed a 55% reduction in the tumor-to-muscle binding ratio of **[^{18}F]3a** from 4.0 to 1.8 at this time interval and also reduced radioligand accumulation in organs known to contain σ receptors such as liver, spleen and lung. Blockade of tumor radioactivity was however less pronounced at 1.5 h (25%) which may be related to its lower specific binding fraction. A possible explanation for the improved blockade observed at 3.5 h versus 1.5 h could be due to improved σ receptor specific binding and higher blood clearance of non-specific binding at later time intervals resulting in improved specific to non-specific binding ratios. It is also conceivable that haloperidol pretreatment (instead of co-injection as in this study) may be more effective at σ receptor blockade at earlier time intervals as demonstrated in other σ receptor radioligand studies.[40-42]

The cell binding studies conducted with **[^{18}F]3a** showed that cell membrane associated radioactivity peaked at 15 min while the internalized component peaked at 30 min post-incubation. The efflux of **[^{18}F]3a** from PC-3 cells was continuous over the 3 h monitoring time (~25% at 3 h post incubation). These results may explain the slight decrease in tumor uptake observed with PET imaging at 3.5 h post-injection. The observation that the decrease in tumor uptake is lower than that seen in the cell studies could be due to the higher cell density present in tumors compared to that in cell suspensions.

Our *in vitro* mouse liver microsomal stability data shows a relatively fast metabolic degradation for **3a** ($T_{½}$ = 5.94 min) which is in contrast with the tumor uptake for **[^{18}F]3a** seen in the PET images. For example, **[^{18}F]3a** associated tumor radioactivity showed a steady accumulation in tumor with a peak uptake of 4.4% ID/g at 1.5 h post-injection despite the fast metabolic degradation predicted by the *in vitro* liver microsomal studies. A possible explanation

is that *in vitro* liver microsome studies may not completely reflect their *in vivo* behavior as previously noted.[43] Furthermore, our plasma analysis data shows that intact **[^{18}F]3a** accounts for >99% and 24% of the total radioactivity at 5 min and 30 min p.i. respectively. Hence, the availability of sufficiently high plasma concentrations of intact **[^{18}F]3a** and its slow binding kinetics for tumor accumulation could explain the PET imaging data.

The studies reported herein describe our initial attempts at dual targeting of σ1 and σ2 receptor overexpression in prostate tumors for diagnostic imaging of PCa. Radioligands that target PSMA or GPCR overexpression have received increased attention recently as PCa imaging agents. As an alternate approach, radioligands which target σ receptor overexpression could be useful in patients that display either PSMA-negative[44] or GRPR-negative tumors.[45] Further refinements in this class of σ receptor radioligands include the possibility of substitution of bromine in **3a** with the chemically related iodine atom, to provide either imaging (PET [^{124}I] and SPECT [^{123}I]) or radiotherapeutic ([^{131}I]) capabilities. Future studies to investigate the detailed σ receptor binding/interaction mechanisms for these ligands and further evaluate their SAR are planned. This information could facilitate development of σ receptor ligands with improved affinity, metabolic stability and internalization into σ receptor-positive tumor cells to further improve its tumor retention. Additionally, tethering these radioligands with multimeric structures,[46, 47] or coupling them to specific nanomaterials to utilize the "multivalency effect" (i.e. simultaneous binding to multiple σ receptors to improve binding affinity and tumor targeting specificity),[48, 49] is a possibility to achieve improved σ receptor-positive tumor targeting.

Supporting Information

The supporting information is available free of charge on http://pubs.acs.org for this manuscript, which includes the dynamic PET scan measurement of circulation half-life, HPLC analysis, elemental analysis, and liver microsome metabolic stability data.

ACKNOWLEDGMENTS

This work was supported, in part, by seed grants from the University of Michigan Comprehensive Cancer Center and The Michigan Memorial Phoenix Project at the University of Michigan. Additional support from Elsa U. Pardee Foundation (to H.H.), the NIH P01-CA085878, Jiangsu Government Scholarship for Overseas Studies (to D.Y.), and the National Science Foundation of China (No. 81201696) is gratefully acknowledged. The authors would also like to thank Dr. Christy John (CDER/FDA, Silver Spring, MD) for many helpful discussions during the course of this work. We thank Dr. Peter Scott and Brian Hockley at the University of Michigan Cyclotron/PET facility for providing 2-[^{18}F]fluoroethyl tosylate.

REFERENCES

(1) Bauman, G.; Belhocine, T.; Kovacs, M.; Ward, A.; Beheshti, M.; Rachinsky, I. ^{18}F-fluorocholine for prostate cancer imaging: a systematic review of the literature. *Prostate Cancer Prostatic Dis.* **2012,** *15*, 45-55.

(2) Roivainen, A.; Kahkonen, E.; Luoto, P.; Borkowski, S.; Hofmann, B.; Jambor, I.; Lehtio, K.; Rantala, T.; Rottmann, A.; Sipila, H.; Sparks, R.; Suilamo, S.; Tolvanen, T.; Valencia, R.; Minn, H. Plasma pharmacokinetics, whole-body distribution, metabolism, and radiation dosimetry of ^{68}Ga bombesin antagonist BAY 86-7548 in healthy men. *J. Nucl. Med.* **2013,** *54*, 867-72.

(3) Mansi, R.; Minamimoto, R.; Macke, H.; Iagaru, A. H. Bombesin-targeted PET of prostate cancer. *J. Nucl. Med.* **2016,** *57*, 67s-72s.

(4) Wieser, G.; Mansi, R.; Grosu, A. L.; Schultze-Seemann, W.; Dumont-Walter, R. A.; Meyer, P. T.; Maecke, H. R.; Reubi, J. C.; Weber, W. A. Positron emission tomography (PET) imaging of prostate cancer with a gastrin releasing peptide receptor antagonist--from mice to men. *Theranostics* **2014,** *4*, 412-9.

(5) Sah, B. R.; Burger, I. A.; Schibli, R.; Friebe, M.; Dinkelborg, L.; Graham, K.; Borkowski, S.; Bacher-Stier, C.; Valencia, R.; Srinivasan, A.; Hany, T. F.; Mu, L.; Wild, P. J.; Schaefer, N. G. Dosimetry and first clinical evaluation of the new ^{18}F-radiolabeled bombesin analogue BAY 864367 in patients with prostate cancer. *J. Nucl. Med.* **2015,** *56*, 372-8.

(6) Minner, S.; Wittmer, C.; Graefen, M.; Salomon, G.; Steuber, T.; Haese, A.; Huland, H.; Bokemeyer, C.; Yekebas, E.; Dierlamm, J.; Balabanov, S.; Kilic, E.; Wilczak, W.; Simon, R.; Sauter, G.; Schlomm, T. High level PSMA expression is associated with early PSA recurrence in surgically treated prostate cancer. *Prostate* **2011,** *71*, 281-8.

(7) Dietlein, M.; Kobe, C.; Kuhnert, G.; Stockter, S.; Fischer, T.; Schomacker, K.; Schmidt, M.; Dietlein, F.; Zlatopolskiy, B. D.; Krapf, P.; Richarz, R.; Neubauer, S.; Drzezga, A.; Neumaier, B. Comparison of [^{18}F]DCFPyL and [^{68}Ga]Ga-PSMA-HBED-CC for PSMA-PET imaging in patients with relapsed prostate cancer. *Mol. Imaging Biol.* **2015,** *17*, 575-84.
(8) Vilner, B. J.; John, C. S.; Bowen, W. D. Sigma-1 and sigma-2 receptors are expressed in a wide variety of human and rodent tumor cell lines. *Cancer Res.* **1995,** *55*, 408-13.
(9) Bem, W. T.; Thomas, G. E.; Mamone, J. Y.; Homan, S. M.; Levy, B. K.; Johnson, F. E.; Coscia, C. J. Overexpression of sigma receptors in nonneural human tumors. *Cancer Res.* **1991,** *51*, 6558-62.
(10) John, C. S.; Vilner, B. J.; Geyer, B. C.; Moody, T.; Bowen, W. D. Targeting sigma receptor-binding benzamides as in vivo diagnostic and therapeutic agents for human prostate tumors. *Cancer Res.* **1999,** *59*, 4578-83.
(11) Hashimoto, K.; Ishiwata, K. Sigma receptor ligands: possible application as therapeutic drugs and as radiopharmaceuticals. *Curr. Pharm. Des.* **2006,** *12*, 3857-76.
(12) Niitsu, T.; Iyo, M.; Hashimoto, K. Sigma-1 receptor agonists as therapeutic drugs for cognitive impairment in neuropsychiatric diseases. *Curr. Pharm. Des.* **2012,** *18*, 875-83.
(13) Hayashi, T.; Su, T. P. Sigma-1 receptor chaperones at the ER-mitochondrion interface regulate Ca^{2+} signaling and cell survival. *Cell* **2007,** *131*, 596-610.
(14) Xu, J.; Zeng, C.; Chu, W.; Pan, F.; Rothfuss, J. M.; Zhang, F.; Tu, Z.; Zhou, D.; Zeng, D.; Vangveravong, S.; Johnston, F.; Spitzer, D.; Chang, K. C.; Hotchkiss, R. S.; Hawkins, W. G.; Wheeler, K. T.; Mach, R. H. Identification of the PGRMC1 protein complex as the putative sigma-2 receptor binding site. *Nat. Commun.* **2011,** *2*, 380.
(15) Abate, C.; Niso, M.; Infantino, V.; Menga, A.; Berardi, F. Elements in support of the 'non-identity' of the PGRMC1 protein with the sigma2 receptor. *Eur. J. Pharmacol.* **2015,** *758*, 16-23.
(16) Chu, U. B.; Mavlyutov, T. A.; Chu, M. L.; Yang, H.; Schulman, A.; Mesangeau, C.; McCurdy, C. R.; Guo, L. W.; Ruoho, A. E. The Sigma-2 receptor and progesterone receptor membrane component 1 are different binding sites derived from independent genes. *EBioMedicine* **2015,** *2*, 1806-13.
(17) Mach, R. H.; Smith, C. R.; al-Nabulsi, I.; Whirrett, B. R.; Childers, S. R.; Wheeler, K. T. Sigma 2 receptors as potential biomarkers of proliferation in breast cancer. *Cancer Res.* **1997,** *57*, 156-61.
(18) Katz, J. L.; Su, T. P.; Hiranita, T.; Hayashi, T.; Tanda, G.; Kopajtic, T.; Tsai, S. Y. A role for sigma receptors in stimulant self administration and addiction. *Pharmaceuticals (Basel)* **2011,** *4*, 880-914.
(19) Banister, S. D.; Kassiou, M. The therapeutic potential of sigma (sigma) receptors for the treatment of central nervous system diseases: evaluation of the evidence. *Curr. Pharm. Des.* **2012,** *18*, 884-901.
(20) Brune, S.; Pricl, S.; Wunsch, B. Structure of the sigma1 receptor and its ligand binding site. *J. Med. Chem.* **2013,** *56*, 9809-19.
(21) van Waarde, A.; Rybczynska, A. A.; Ramakrishnan, N. K.; Ishiwata, K.; Elsinga, P. H.; Dierckx, R. A. Potential applications for sigma receptor ligands in cancer diagnosis and therapy. *Biochim. Biophys. Acta.* **2015,** *1848*, 2703-14.
(22) Huang, Y. S.; Lu, H. L.; Zhang, L. J.; Wu, Z. Sigma-2 receptor ligands and their perspectives in cancer diagnosis and therapy. *Med. Res. Rev.* **2014,** *34*, 532-66.
(23) Everaert, H.; Flamen, P.; Franken, P. R.; Verhaeghe, W.; Bossuyt, A. Sigma-receptor imaging by means of I123-IDAB scintigraphy: clinical application in melanoma and non-small cell lung cancer. *Anticancer Res.* **1997,** *17*, 1577-82.
(24) Moura, C.; Gano, L.; Mendes, F.; Raposinho, P. D.; Abrantes, A. M.; Botelho, M. F.; Santos, I.; Paulo, A. ^{99m}Tc(I)/Re(I) tricarbonyl complexes for in vivo targeting of melanotic melanoma: Synthesis and biological evaluation. *Eur. J. Med. Chem.* **2012,** *50*, 350-60.
(25) Shoghi, K. I.; Xu, J.; Su, Y.; He, J.; Rowland, D.; Yan, Y.; Garbow, J. R.; Tu, Z.; Jones, L. A.; Higashikubo, R.; Wheeler, K. T.; Lubet, R. A.; Mach, R. H.; You, M. Quantitative receptor-based imaging of tumor proliferation with the sigma-2 ligand [^{18}F]ISO-1. *PLoS One* **2013,** *8*, e74188.
(26) Tu, Z.; Xu, J.; Jones, L. A.; Li, S.; Zeng, D.; Kung, M. P.; Kung, H. F.; Mach, R. H. Radiosynthesis and biological evaluation of a promising sigma2-receptor ligand radiolabeled with fluorine-18 or iodine-125 as a PET/SPECT probe for imaging breast cancer. *Appl. Radiat. Isot.* **2010,** *68*, 2268-73.

(27) Tu, Z.; Dence, C. S.; Ponde, D. E.; Jones, L.; Wheeler, K. T.; Welch, M. J.; Mach, R. H. Carbon-11 labeled sigma2 receptor ligands for imaging breast cancer. *Nucl. Med. Biol.* **2005,** *32*, 423-30.
(28) Li, D.; Chen, Y.; Wang, X.; Deuther-Conrad, W.; Chen, X.; Jia, B.; Dong, C.; Steinbach, J.; Brust, P.; Liu, B.; Jia, H. ^{99m}Tc-cyclopentadienyl tricarbonyl chelate-labeled compounds as selective sigma-2 receptor ligands for tumor imaging. *J. Med. Chem.* **2016,** *59*, 934-46.
(29) Colabufo, N. A.; Abate, C.; Contino, M.; Inglese, C.; Niso, M.; Berardi, F.; Perrone, R. PB183, a sigma receptor ligand, as a potential PET probe for the imaging of prostate adenocarcinoma. *Bioorg. Med. Chem. Lett.* **2008,** *18*, 1990-3.
(30) Selivanova, S. V.; Toscano, A.; Abate, C.; Berardi, F.; Muller, A.; Kramer, S. D.; Schibli, R.; Ametamey, S. M. Synthesis and pharmacological evaluation of ^{11}C-labeled piperazine derivative as a PET probe for sigma-2 receptor imaging. *Nucl. Med. Biol.* **2015,** *42*, 399-405.
(31) van Waarde, A.; Rybczynska, A. A.; Ramakrishnan, N.; Ishiwata, K.; Elsinga, P. H.; Dierckx, R. A. Sigma receptors in oncology: therapeutic and diagnostic applications of sigma ligands. *Curr. Pharm. Des.* **2010,** *16*, 3519-37.
(32) Jacobson, O.; Kiesewetter, D. O.; Chen, X. Fluorine-18 radiochemistry, labeling strategies and synthetic routes. *Bioconjug. Chem.* **2015,** *26*, 1-18.
(33) Huang, C.; McConathy, J. Fluorine-18 labeled amino acids for oncologic imaging with positron emission tomography. *Curr. Top. Med. Chem.* **2013,** *13*, 871-91.
(34) Wilson, A. A.; Dasilva, J. N.; Houle, S. Synthesis of two radiofluorinated cocaine analogues using distilled 2-[^{18}F]fluoroethyl bromide. *Appl. Radiat. Isot.* **1995,** *46*, 765-70.
(35) Musachio, J. L.; Lever, J. R. Vinylstannylated alkylating agents as prosthetic groups for radioiodination of small molecules: design, synthesis, and application to iodoallyl analogues of spiperone and diprenorphine. *Bioconjug. Chem.* **1992,** *3*, 167-75.
(36) Tu, Z.; Xu, J.; Jones, L. A.; Li, S.; Dumstorff, C.; Vangveravong, S.; Chen, D. L.; Wheeler, K. T.; Welch, M. J.; Mach, R. H. Fluorine-18-labeled benzamide analogues for imaging the sigma2 receptor status of solid tumors with positron emission tomography. *J. Med. Chem.* **2007,** *50*, 3194-204.
(37) Ogawa, K.; Kanbara, H.; Shiba, K.; Kitamura, Y.; Kozaka, T.; Kiwada, T.; Odani, A. Development and evaluation of a novel radioiodinated vesamicol analog as a sigma receptor imaging agent. *EJNMMI Res.* **2012,** *2*, 54.
(38) Patel, S.; Gibson, R. In vivo site-directed radiotracers: a mini-review. *Nucl. Med. Biol.* **2008,** *35*, 805-15.
(39) Arnott, J. A.; Planey, S. L. The influence of lipophilicity in drug discovery and design. *Expert Opin. Drug Discov.* **2012,** *7*, 863-75.
(40) Wang, X.; Li, Y.; Deuther-Conrad, W.; Xie, F.; Chen, X.; Cui, M. C.; Zhang, X. J.; Zhang, J. M.; Steinbach, J.; Brust, P.; Liu, B. L.; Jia, H. M. Synthesis and biological evaluation of ^{18}F labeled fluoro-oligo-ethoxylated 4-benzylpiperazine derivatives for sigma-1 receptor imaging. *Bioorg. Med. Chem.* **2013,** *21*, 215-22.
(41) Wang, X.; Li, D.; Deuther-Conrad, W.; Lu, J.; Xie, Y.; Jia, B.; Cui, M.; Steinbach, J.; Brust, P.; Liu, B.; Jia, H. Novel cyclopentadienyl tricarbonyl ^{99m}Tc complexes containing 1-piperonylpiperazine moiety: potential imaging probes for sigma-1 receptors. *J. Med. Chem.* **2014,** *57*, 7113-25.
(42) Kawamura, K.; Ishiwata, K.; Tajima, H.; Ishii, S.; Matsuno, K.; Homma, Y.; Senda, M. In vivo evaluation of [^{11}C]SA4503 as a PET ligand for mapping CNS sigma1 receptors. *Nucl. Med. Biol.* **2000,** *27*, 255-61.
(43) Wienkers, L. C.; Heath, T. G. Predicting in vivo drug interactions from in vitro drug discovery data. *Nat. Rev. Drug Discov.* **2005,** *4*, 825-33.
(44) Maurer, T.; Gschwend, J. E.; Rauscher, I.; Souvatzoglou, M.; Haller, B.; Weirich, G.; Wester, H. J.; Heck, M.; Kubler, H.; Beer, A. J.; Schwaiger, M.; Eiber, M. Diagnostic efficacy of ^{68}Gallium-PSMA positron emission tomography compared to conventional imaging for lymph node staging of 130 consecutive patients with intermediate to high risk prostate cancer. *J. Urol.* **2016,** *195*, 1436-43.
(45) Beer, M.; Montani, M.; Gerhardt, J.; Wild, P. J.; Hany, T. F.; Hermanns, T.; Muntener, M.; Kristiansen, G. Profiling gastrin-releasing peptide receptor in prostate tissues: clinical implications and molecular correlates. *Prostate* **2012,** *72*, 318-25.

(46) Li, W.; Lang, L.; Niu, G.; Guo, N.; Ma, Y.; Kiesewetter, D. O.; Shen, B.; Chen, X. N-Succinimidyl 4-[^{18}F]-fluoromethylbenzoate-labeled dimeric RGD peptide for imaging tumor integrin expression. *Amino Acids* **2012,** *43*, 1349-57.
(47) Zhang, Y.; Huang, Y.; Zhang, P.; Gao, X.; Gibbs, R. B.; Li, S. Incorporation of a selective sigma-2 receptor ligand enhances uptake of liposomes by multiple cancer cells. *Int. J. Nanomedicine* **2012,** *7*, 4473-85.
(48) Sun, X.; Cai, W.; Chen, X. Positron emission tomography imaging using radiolabeled inorganic nanomaterials. *Acc. Chem. Res.* **2015,** *48*, 286-94.
(49) Yan, Y.; Chen, X. Peptide heterodimers for molecular imaging. *Amino Acids* **2011,** *41*, 1081-92.

FIGURE LEGENDS

Scheme 1 Synthesis of compound **3a** and **3b**.

Scheme 2 Synthesis of compound **7a** and **7b**.

Scheme 3 Synthesis of **[^{18}F]3a**.

Figure 1 Design Strategy for Dual SR-targeting Ligands

Figure 2 Interaction of **[^{18}F]3a** with SR-positive PC-3 cells. Cell surface-bound **(A);** Internalized **(B);** Efflux rate **(C)** of **[^{18}F]3a** after PC-3 cell internalization.

Figure 3 *In vivo* PET studies using **[^{18}F]3a** in PC-3 tumor bearing mice. (A) Representative coronal PET images of PC-3 tumor-bearing mice at 15 min, 1.5, and 3.5 h post-injection of **[^{18}F]3a** and **^{18}F]3a** co-injected with haloperidol (i.e. blocking group). Yellow arrowheads indicate tumor location. Time-activity curves of U87MG tumor, liver, blood, and muscle are also shown upon injection of (B) **[^{18}F]3a** (n = 3) and (C) **[^{18}F]3a** with blocking (n = 3). (D) Comparison of PC-3 tumor uptake in **[^{18}F]3a** and blocking group. * $P<0.05$.

Figure 4 *Ex vivo* evaluation of **[^{18}F]3a**. (A) Organ distribution profile of **[^{18}F]3a** and blocking group at 1.5 h post-injection and 3.5 h post-injection in PC-3 tumor-bearing mice. Blocking data was only shown at 3.5 h p.i. (B) Immunohistological staining of PC-3 tumor, kidney, liver, and muscle to confirm the expression level of $\sigma_1 + \sigma_2$ receptors. Magnitude: 200×. Scale bar: 50 μm.

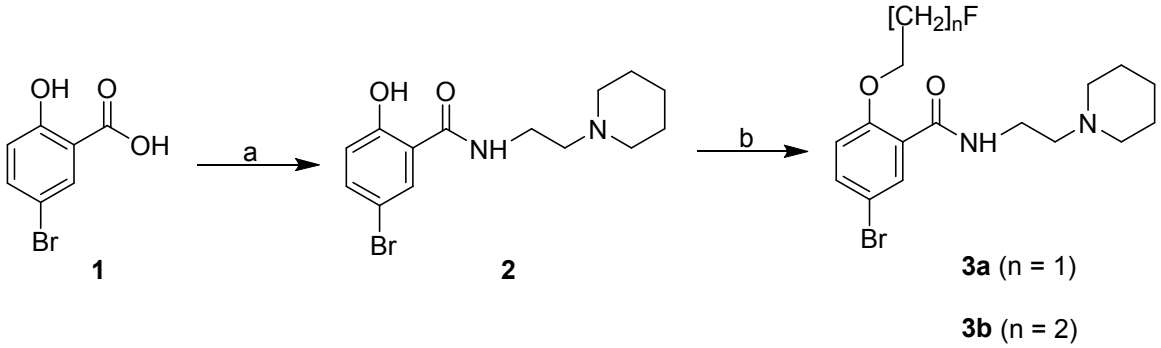

[a]**Reagents and conditions**: (a) 1. $SOCl_2$, $CHCl_3$, reflux, 2. *N*-(2-aminoethyl)piperidine, Et_3N, toluene/DMF, rt, 62%; (b) TBAOH, F-$[CH_2]_n$-OTos (n = 2, 3), DMF, 65 ^{0}C, 57 - 61%.

Scheme 1

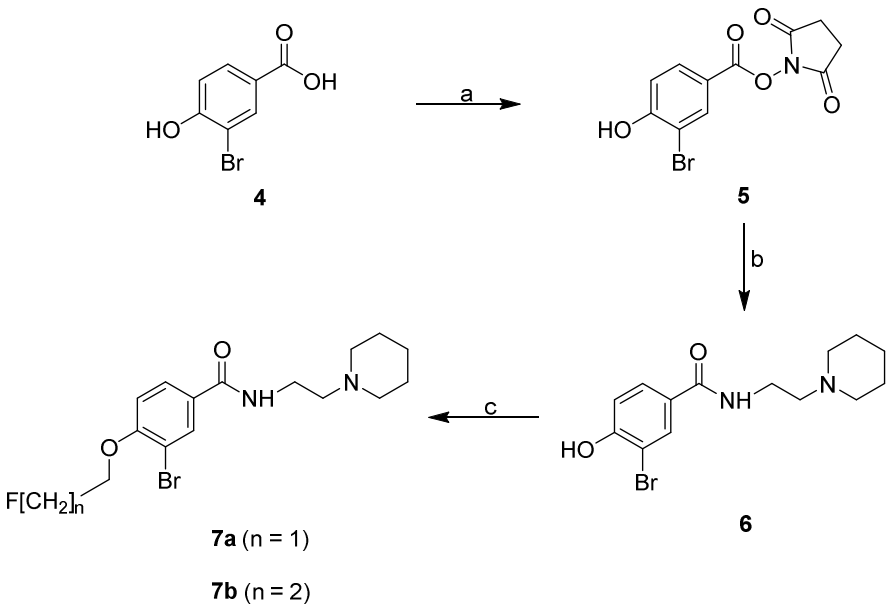

[a]**Reagents and conditions**: (a) *N,N'*-disuccinimidyl carbonate, pyridine, CH_3CN, rt, 88%; (b) *N*-(2-aminoethyl)piperidine, CH_2Cl_2, rt, 71%; (c) TBAOH, F-$[CH_2]_n$-OTos (n = 2, 3), DMF, 65 ^{0}C, 89 - 90%.

Scheme 2

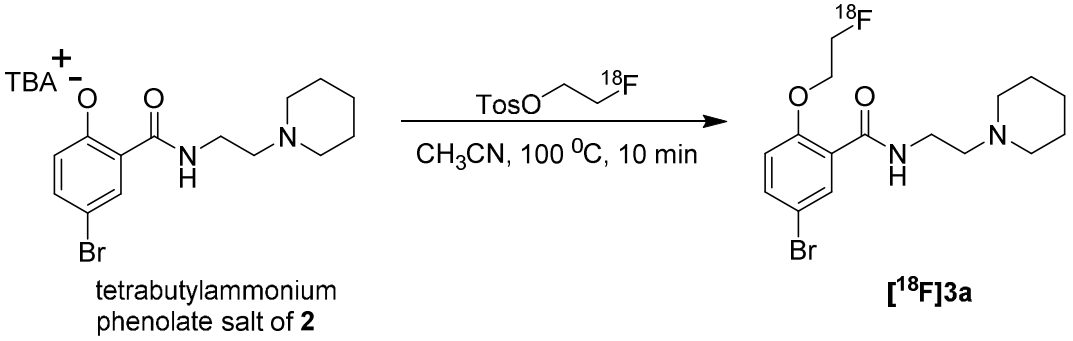

Scheme 3

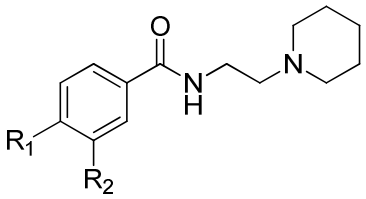

			K_i (nM)	
Compound	**R_1**	**R_2**	**σ_1**	**σ_2**
4-IPAB	I	H	2.57 ± 0.70	205 ± 67
PIMBA	CH_3O	I	11.82 ± 0.68	206 ± 11

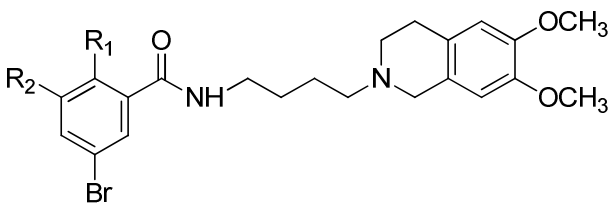

			K_i (nM)	
Compound	**R_1**	**R_2**	**σ_1**	**σ_2**
8	FCH_2CH_2O	H	1076 ± 88	0.65 ± 0.22
9	CH_3O	CH_3O	12,900 ± 111	8.2 ± 1.4

Figure 1

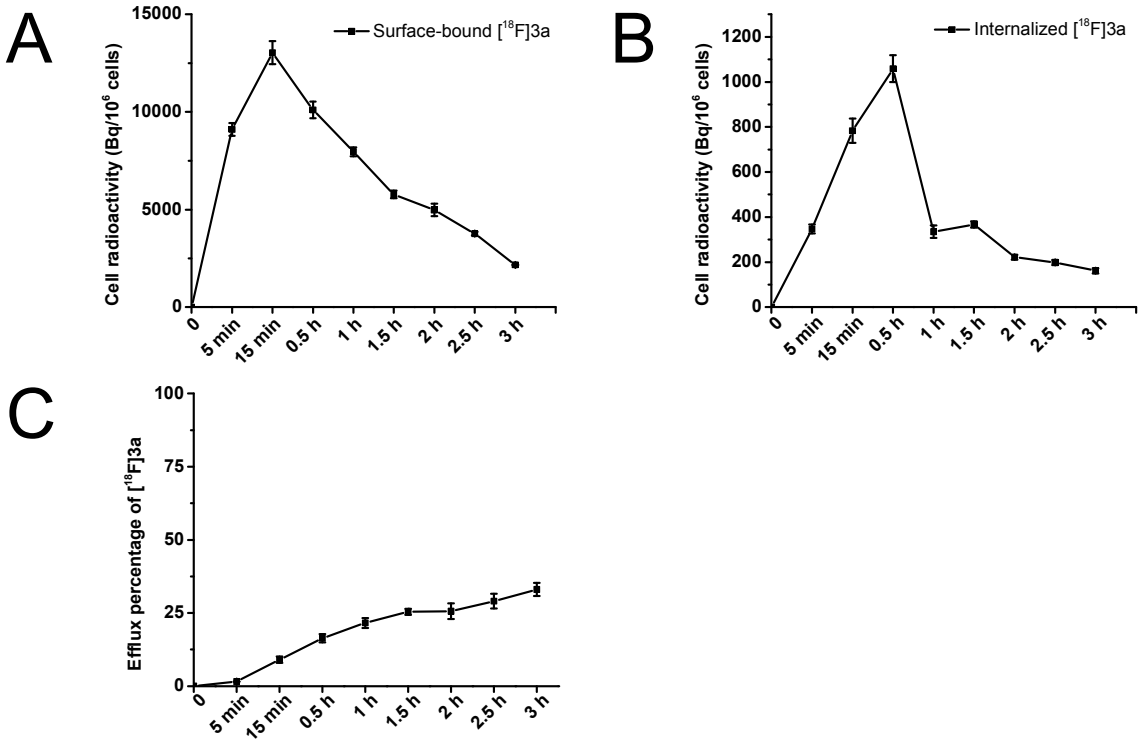
A
Surface-bound [18F]3a
Cell radioactivity (Bq/10^6 cells)
15000
10000
5000
0
0
5 min
15 min
0.5 h
1 h
1.5 h
2 h
2.5 h
3 h
B
Internalized [18F]3a
Cell radioactivity (Bq/10^6 cells)
1200
1000
800
600
400
200
0
C
Efflux percentage of [18F]3a
100
75
50
25
0

Figure 2

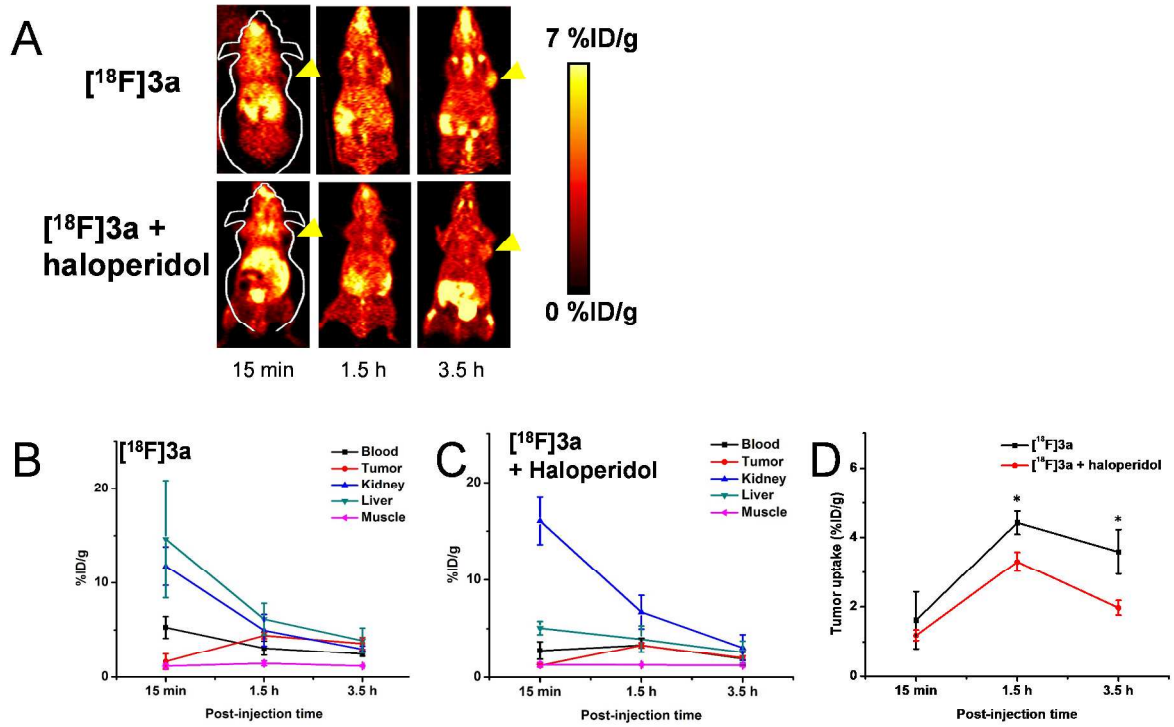

Figure 3

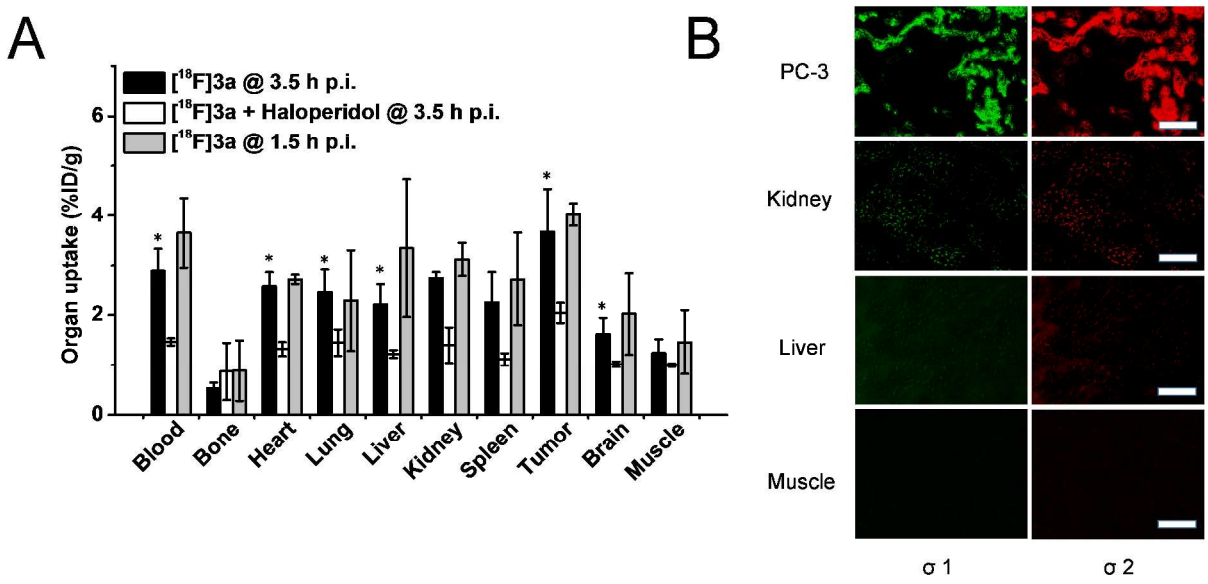

Figure 4

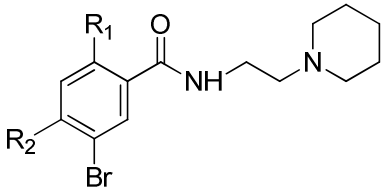

Table 1 *In Vitro* Binding Affinity (K_i) Data of Benzamide Derivatives for Sigma Receptor Subtypes

Ligands	R_1	R_2	K_i (nM) σ_1	K_i (nM) σ_2	[a]cLogP	[b]cLogD
3a	FCH_2CH_2O-	H	6.26 ± 1.0	10.2 ± 1.0	2.8	1.4
3b	$FCH_2CH_2CH_2O$-	H	52.9 ± 17	92.9 ± 64	2.9	2.1
7a	H	FCH_2CH_2O-	36.1 ± 20	42.8 ± 14	2.8	1.9
7b	H	$FCH_2CH_2CH_2O$-	23.3 ± 6	28.3 ± 21	2.9	2.0
2	OH	H	> 10,000	> 10,000	2.3	2.0
6	H	OH	> 10,000	> 10,000	2.3	1.2
Haloperidol	-	-	5.0 ± 1.7[c]	20.7 ± 0.1[c]	-	-

[a]cLogP data were obtained using ChemDraw Professional (version 15.0.0.106)

[b]cLogD data (pH 7.4) were obtained using ChemAxon Calculator Plugin

[c]Data from Reference[40]

For Table Of Contents Use Only

Design and Investigation of a [^{18}F]-labeled Benzamide Derivative as a High Affinity Dual Sigma Receptor Subtype Radioligand for Prostate Tumor Imaging

Dongzhi Yang[1,2], Anthony Comeau[3], Wayne D. Bowen[3], Robert H. Mach[4], Brian D. Ross[1], Hao Hong[1], Marcian E. Van Dort[1]

[1] Center for Molecular Imaging, Department of Radiology, University of Michigan – Ann Arbor, Michigan 48109-2200, United States

[2] Jiangsu Key Laboratory of New Drug Research and Clinical Pharmacy, Xuzhou Medical University, Xuzhou, Jiangsu 221004, China

[3] Department of Molecular Pharmacology, Physiology & Biotechnology, Brown University, Providence, RI 02912, United States

[4] Department of Radiology, University of Pennsylvania, Philadelphia, PA 19104, United States